Princeton Plasma Physics Laboratory

PPPL- 4795

PPPL- 4795

# Bootstrap Current for the Edge Pedestal Plasma in a Diverted Tokamak Geometry

S. Koh, C.S. Chang, S. Ku, J.E. Menard, H. Weitzner and W. Choe

August, 2012

PPPL PRINCETON PLASMA PHYSICS LABORATORY

Prepared for the U.S. Department of Energy under Contract DE-AC02-09CH11466.

# Princeton Plasma Physics Laboratory
# Report Disclaimers

---

## Full Legal Disclaimer



## Trademark Disclaimer



---

# PPPL Report Availability

## Princeton Plasma Physics Laboratory:

http://www.pppl.gov/techreports.cfm

## Office of Scientific and Technical Information (OSTI):

http://www.osti.gov/bridge

---

**Related Links:**

**U.S. Department of Energy**

**Office of Scientific and Technical Information**

**Fusion Links**

# Bootstrap current for the edge pedestal plasma in a diverted tokamak geometry

S. Koh,[1] C. S. Chang,[2] S. Ku,[2] J. E. Menard,[2] H. Weitzner,[3] and W. Choe[1]
[1]*Korea Advanced Institute of Science and Technology, Department of Physics, Daejeon 305-701, Korea*
[2]*Princeton Plasma Physics Laboratory, Princeton University, Princeton, New Jersey 08543, USA*
[3]*Courant Institute of Mathematical Sciences, New York University, New York, New York 10012, USA*

(Received 20 March 2012; accepted 6 June 2012; published online 12 July 2012)

The edge bootstrap current plays a critical role in the equilibrium and stability of the steep edge pedestal plasma. The pedestal plasma has an unconventional and difficult neoclassical property, as compared with the core plasma. It has a narrow passing particle region in velocity space that can be easily modified or destroyed by Coulomb collisions. At the same time, the edge pedestal plasma has steep pressure and electrostatic potential gradients whose scale-lengths are comparable with the ion banana width, and includes a magnetic separatrix surface, across which the topological properties of the magnetic field and particle orbits change abruptly. A drift-kinetic particle code XGC0, equipped with a mass-momentum-energy conserving collision operator, is used to study the edge bootstrap current in a realistic diverted magnetic field geometry with a self-consistent radial electric field. When the edge electrons are in the weakly collisional banana regime, surprisingly, the present kinetic simulation confirms that the existing analytic expressions [represented by O. Sauter *et al.*, Phys. Plasmas **6**, 2834 (1999)] are still valid in this unconventional region, except in a thin radial layer in contact with the magnetic separatrix. The agreement arises from the dominance of the electron contribution to the bootstrap current compared with ion contribution and from a reasonable separation of the trapped-passing dynamics without a strong collisional mixing. However, when the pedestal electrons are in plateau-collisional regime, there is significant deviation of numerical results from the existing analytic formulas, mainly due to large effective collisionality of the passing and the boundary layer trapped particles in edge region. In a conventional aspect ratio tokamak, the edge bootstrap current from kinetic simulation can be significantly less than that from the Sauter formula if the electron collisionality is high. On the other hand, when the aspect ratio is close to unity, the collisional edge bootstrap current can be significantly greater than that from the Sauter formula. Rapid toroidal rotation of the magnetic field lines at the high field side of a tight aspect-ratio tokamak is believed to be the cause of the different behavior. A new analytic fitting formula, as a simple modification to the Sauter formula, is obtained to bring the analytic expression to a better agreement with the edge kinetic simulation results. © *2012 American Institute of Physics*.
[http://dx.doi.org/10.1063/1.4736953]

## I. INTRODUCTION

The importance of the bootstrap current in tokamak plasma operation has been well recognized as a critical component in characterizing the plasma and the magnetic field equilibrium for developing advanced steady state operation scenarios, and for understanding neoclassical tearing modes.[1–6] Existing studies of the bootstrap current and the construction of analytic formulas being used in the equilibrium and stability analyses have been mainly focused on the core plasma.[7–10] Recently, the importance of the bootstrap current has been re-emphasized through its critical role played in the stability, equilibrium, and turbulence studies of the steep gradient edge pedestal[13,14] in H-mode (high confinement mode) operation. A steep pressure gradient in the edge pedestal yields a large localized bootstrap current. Inaccuracy in the bootstrap current formula in the edge region, which could have been considered to be of small consequence to the overall plasma current profile in the previous core-oriented formulation, may now be amplified and become critical. A more accurate evaluation of the bootstrap current profile in the edge region of tokamak plasma is needed. Kagan and Catto[15] studied the ion flow aspect of the problem in the large aspect ratio limit, arising from the interaction of finite ion banana width with the strong radial electric field occurring in the edge pedestal.

While most other transport phenomena in tokamak plasma are dominated by turbulence physics, the parallel plasma current has been experimentally validated to obey neoclassical physics.[16–20] The neoclassical bootstrap current arises from the particle orbit excursion across radial pressure gradient. It has been known that source of the current is mostly the trapped particles, but the current is carried mostly by the passing particles via collisional coupling between trapped and passing particles. There is a transitional boundary layer between the trapped and passing regions in velocity space, which plays an important role in determining the magnitude of the bootstrap current.[9] It is necessary to improve

 

the bootstrap current formula for application in edge pedestal plasma as the neoclassical physics in the edge plasma is unconventional and difficult, compared to the core plasma. Specifically, the edge pedestal plasma has a narrow passing particle (current carrier) region in velocity space, which can be easily modified or destroyed by Coulomb collisions, while the formulation of the conventional bootstrap current has been focused on the core plasma and is based upon the collisional modification of the "effective trapped particle fraction," which plays a dominant role in the behavior of the bootstrap current in a conventional core plasma. Since the Coulomb collisionality varies widely across the steep pressure gradient in the pedestal layer, a single collisionality limit approximation is not reasonable in the study of pedestal physics. The edge pedestal plasma has a steep gradient, whose scale length is similar to the ion banana width, so that one must include the nonlinear interaction between the ion radial excursion and the plasma pressure gradient. The existing formulas are based upon linearized approximation under the assumption that the radial banana excursion width is much smaller than the plasma pressure gradient scale length. Moreover, the pedestal plasma contains a magnetic separatrix surface, across which the bootstrap-current generating topological property of particle orbits change abruptly. This is another finite radial excursion effect which has not been considered in the previous bootstrap current theories and simulations. The difference between the two opposite vertical magnetic drift directions may appear from this effect in a thin radial layer in contact with the magnetic separatrix surface. Another physics effect not recognized in the previous theories is the extreme largeness of the toroidal magnetic field component compared to the poloidal component at the high field side, as the toroidal aspect ratio becomes small. Many trapped particles then execute multiple toroidal rotations at the high field side before they recognize that they are in the trapped particle regime. Under strong pitch-angle collisions, these particles are virtually indistinguishable with the passing particles. As a result, the effective passing particle fraction can be higher in a tight aspect ratio tokamak edge.

The bootstrap current can be evaluated from solution of the drift kinetic equation

$$\partial f/\partial t + (\vec{v}_{\|} + \vec{v}_d) \cdot \nabla f = C(f,f),$$

as has been studied in previous kinetic calculations using the linearized version of this equation. Here, the Ohmic loop voltage drive is omitted for simplicity ($E_{\|} = 0$), $\vec{v}_d$ is the drift velocity from $\nabla B$, magnetic curvature and radial electric field effects, and $C$ is the Coulomb collision operator. Contribution to the flux-surface-averaged bootstrap current from the variation of the electrostatic potential $\Phi$ on magnetic surface enters in the form $\langle \vec{B} \cdot \nabla \Phi \rangle$,[9] which is identically zero except for the small inductive contribution being neglected here. This property enables the flux-surface-averaged bootstrap current evaluation using the flux-function $\langle \Phi \rangle$.

In this study, the drift-kinetic particle code XGC0, equipped with a mass-momentum-energy conserving collision operator, solves the above drift kinetic equation for the bootstrap current $\mathbf{J}_b$. In order to include the edge effect faithfully, the simulation is performed in realistic diverted geometry with the self-consistent neoclassical solution for $\langle \Phi \rangle$, unlike in the previous studies. Another difference of the present study from the existing theories is that we solve the Vlasov part (left hand side of the above equation) in its original form without linearization in banana width, in order to include the finite orbit excursion effects in the steep radial gradient of plasma pressure and electrostatic potential $\langle \Phi \rangle$, and in the magnetic separatrix geometry. The Coulomb collision operator used in the present study is, however, linearized, and is similar to that used in the most popular study by Sauter *et al.*[10] The kinetic simulation has been verified against the existing formula of Ref. 10 in its confidence regime, i.e., tokamak core plasma with high toroidal aspect ratio $r/R \lesssim 0.2$ (the validity verification of the Sauter's analytic formula in Ref. 10 against their numerical simulation was limited to this aspect ratio, corresponding to the collisionless trapped particle fraction of 0.65 or less). In the zero banana width limit, Sauter *et al.*[10] used the bounce averaged CQL3D code[11] for accurate evaluation of the linearized drift kinetic equation in the collisionless limit, and CQLP (Ref. 12) for the collisionality dependence in realistic core geometry without magnetic separatrix. Their analytic fitting formula was then developed to be within 5% of their code results under the "usual" plasma condition. As the bootstrap current becomes large in the steep edge pedestal ($r/R \gtrsim 0.3$, corresponding to trapped fraction of 0.75 or higher), surprisingly, it is found that the present numerical results still trace Sauter formula reasonably closely for $\psi_N < 0.99$ if the effective collisionality of the passing electrons is low. Here, $\psi_N$ is the poloidal magnetic flux normalized to be unity at the separatrix and zero at the magnetic axis. However, it is found that at higher electron collisionality, the numerically obtained bootstrap current in the steep edge pedestal can be significantly greater than the Sauter formula result in a tight aspect ratio tokamak such as NSTX[21] and can be significantly smaller than the Sauter formula in a conventional aspect ratio tokamak such as DIII-D[22] and C-Mod.[23] A simple modification to the Sauter formula has been obtained to bring the analytic fitting formula to a better agreement with the present results in the edge pedestal.

The drift-kinetic code XGC0 is briefly summarized in Sec. II, followed by the presentation of the numerical results in Sec. III. A simple improvement to the Sauter formula is presented in Sec. IV. Application of the present formula, and the Sauter formula, to an impure ion plasma is discussed in Sec. V. Section VI contains conclusion and discussion.

## II. THE XGC0 CODE

XGC0 is a drift-kinetic particle-in-cell code,[24] a turbulence-free version of the gyrokinetic particle code XGC1,[25,26] in which the five-dimensional (3D in position and 2D in velocity) time advance of the marker ion and electron positions is described by the well-known Lagrangian equation of motion,[27] which conserves mass, momentum, and energy:

$$d\mathbf{x}/dt = (1/D)[q\hat{v}_\parallel \mathbf{B}/m + (q\hat{v}_\parallel^2)\nabla \times \mathbf{B} + \mathbf{B} \times \nabla H/B^2],$$
$$d\hat{v}_\parallel/dt = -(1/B^2 D)[\nabla \cdot \mathbf{B} + \hat{v}_\parallel \nabla H \cdot \nabla \times \mathbf{B}],$$
$$d\mu/dt = 0,$$

where $H$ is the Hamiltonian $H = (q/2m)\hat{v}_\parallel^2 \mathbf{B}^2 + \mu B/q + \langle\Phi\rangle$, $\hat{v}_\parallel = mv_\parallel/qB$ is the normalized parallel speed, $D = 1 + \hat{v}_\parallel \mathbf{B} \cdot \nabla \times \mathbf{B}/B^2$ is the Jacobian in the canonical phase space, $\mathbf{X}$ is the marker particle position, $q$ is the charge number, $m$ is the mass, $\mathbf{B}$ is the magnetic field vector, and $\mu$ is the magnetic moment.

A special feature in XGC0 and XGC1 is the use of cylindrical coordinate system for advancing the Lagrangian particles, enabling the inclusion of realistic magnetic geometry with magnetic separatrix (and the magnetic X-point). In the so-called "magnetic flux coordinate" system widely used by tokamak core kinetic codes, the equations of motion encounter a mathematical singularity on the magnetic separatrix surface and the error in the particle motion grows rapidly toward it. Thus, the standard magnetic flux coordinate system cannot be used to describe plasma equations of motions in the diverted edge plasma. The electrostatic potential solvers in XGC0 (XGC1) are, however, approximately aligned to the equilibrium flux surfaces (magnetic field lines).

In XGC0, the flux-surface averaged quasi-equilibrium electrostatic potential is obtained using the flux-surface-averaged radial Ampere's law:[28]

$$[\langle|\nabla\psi|^2\rangle + 4\pi n_i m_i c^2 \langle|\nabla\psi|^2/B^2\rangle] \times \partial^2\langle\Phi\rangle/\partial t\partial\psi = 4\pi\langle\mathbf{J}_{NC} \cdot \nabla\psi\rangle, \quad (1)$$

where the small pressure anisotropy of second order in gyroradius has been neglected, $\psi$ is the poloidal magnetic flux, and $\langle\mathbf{J}_{NC} \cdot \nabla\psi\rangle$ is the flux-surface-averaged neoclassical radial guiding center current, without including the classical polarization current separated out as the second term on the left hand side. For a long, experimental time scale simulation in the absence of a three-dimensional magnetic perturbation, second order terms from neoclassical pressure anisotropy may be needed to reach a true steady state solution for $\langle\Phi\rangle$. If a three-dimensional magnetic perturbation exist, even at a small level,[29–31] or neutral atomic collisions exist in the edge pedestal,[32] these effects can easily dominate the second order pressure anisotropy effect. $\langle\mathbf{J}_{NC} \cdot \nabla\psi\rangle$ may exist during the transient period after the equilibrium is perturbed or after the start of the simulation. This transient period lasts for only a few banana motion periods, followed by GAM (geodesic acoustic mode) oscillation and its damping into a neoclassical quasi-equilibrium state. In this sense, our short time solution is called neoclassical "quasi-equilibrium" solution. The above solver equation (1) is valid only in the closed magnetic surface region. In the open field line region, XGC0 takes a simplified approach: On each flux surface volume, the flux-function electrostatic potential is determined by the requirement that the perpendicular drift losses across the magnetic field and the parallel losses to the first wall to combine together to satisfy the ambipolarity condition between ions and electrons. This is a generalization of the logical sheath concept,[33] which considered only the parallel losses of electrons and ions to the wall. As the separatrix is approached from the scrape-off side, the magnetic connection length becomes infinite, the parallel loss vanishes, $\langle\mathbf{J}_{NC} \cdot \nabla\psi\rangle$ determines $\langle\Phi\rangle$ as in Eq. (1), and the potential solution becomes continuous across the separatrix. A toroidal Ampere's law solver library is available in XGC0 to calculate the three-dimensional electromagnetic perturbation caused by external coil arrays (resonant magnetic perturbation), but is not used in this study.

Another special feature in XGC0 is that it does not use the popular perturbed distribution function (delta-*f*) method, which is applicable to a thermodynamically isolated system. The delta-*f* method cannot study edge plasma, which contains the magnetic separatrix surface and the open magnetic field region. The normal full distribution function method used in XGC0 accepts sources and sinks (such as particle loss to the wall, heat source, torque source, neutral ionization, etc.), and allows the background plasma profile evolution driven by the sources/sinks and the radial transport. Heat and torque sources are normally placed at the inner radial boundary to induce heat and torque fluxes into the edge simulation region, or in the core plasma with spatial distributions when a whole volume is simulated. Heating is normally modeled in XGC0 by raising the particle energy, while keeping zero net torque input. A torque source is modeled by shifting the parallel speed of particles by a small fraction of thermal speed, while keeping zero net heat input. In the present simulation, the heat and torque sources are turned off to avoid any possible heat and torque source effects on the bootstrap current, for a fair comparison with previous bootstrap current theories. Effect of the heat and torque source on the bootstrap current, if any, will be a separate topic for a future study. A linear Monte-Carlo Coulomb collision operator is used in the present simulation,[25,34–38] which is similar to that used in the Sauter formulation.[10] The collision operator preserves particle, momentum, and energy conservation features in both intra and inter-species collisions. In a homogeneous, thermally isolated system, this collision operator yields Maxwellian velocity distribution solution. A fully nonlinear Landau collision operation is also available in XGC0. A simple Monte Carlo neutral particle transport routine is embedded in XGC0 using models for ionization and charge exchange cross-sections, with the atomic neutral particle recycling from the lost plasma particles at the wall and from neutral atomic gas puffing source at a poloidal location. For a more complete neutral molecular-atomic transport, DEGAS2 (Ref. 39) is also coupled in as a subroutine. However, neither of the neutral particle transport routines are turned on in the present study for a clear separation of the physics issues: The neutral particle effect on the bootstrap current, if any, is left as a future study subject. Multi-species impurity particles are usually simulated together with a radiative energy loss model, but are not used in the present deuteron plasma study, either. Instead, the deuteron ion charge number has been changed in order to follow and compare with the Sauter's calculation.

## III. NUMERICAL RESULTS

The magnetic field is given as $\vec{\mathbf{B}} = \vec{\mathbf{B}}_P + \vec{\mathbf{B}}_T = \nabla\phi \times \nabla\psi + I\nabla\phi$, with $\phi$ being the toroidal angle and

$I = RB$, and the plasma current density in steady state is given by

$$\vec{J} = -RdP/d\psi\hat{\phi} + K(\psi)\vec{\mathbf{B}},$$

where $K(\psi) = \langle \vec{J} \cdot \vec{\mathbf{B}} \rangle / \langle B^2 \rangle + I/\langle B^2 \rangle dP/d\psi$. It can be easily shown that the flux surface averaged toroidal bootstrap current can be measured as

$$\langle J_{b\phi} B/B_0 \rangle = \langle \vec{J}_b \cdot \vec{B}/B_0 \rangle \langle B_\phi B \rangle / \langle B^2 \rangle, \qquad (2)$$

where the subscript $\phi$ denotes the toroidal component, $\vec{J}$ is the net current density vector, and $B_0$ is the magnetic field magnitude at the magnetic axis. The inductive Ohmic loop voltage, which could be used to determine the neoclassical electrical conductivity, is set to zero in the present study. The toroidal bootstrap current in the large aspect ratio approximation has usually been assumed to be equal to the parallel current $\langle J_{b\|} B/B_0 \rangle$. For a more accurate study, we calculate $\langle J_{b\phi} B/B_0 \rangle$ in this work. However, it is found that the difference between $\langle J_{b\phi} B/B_0 \rangle$ and $\langle J_{b\|} B/B_0 \rangle$ is less than 1% even in the NSTX geometry. Since the fidelity of the electron physics is important in the evaluation of the bootstrap current, the real electron mass is used instead of an artificially enhanced mass. In XGC0, the radial electric field and the ion toroidal/poloidal flows are generated consistently with the edge effects: i.e., steep pedestal plasma profile, magnetic separatrix geometry, and the X-transport phenomenon.[25] The simulation normally uses about 100 millions particles and takes about 6 h on 70 000 Hopper cores at NERSC. The large scale parallel computation is necessary in order to take care of the short electron simulation time step, especially the subcycling in the short collision time step in the collisional edge pedestal plasma.

In consideration of the special edge physics conditions (mainly, the high sensitivity of passing particle dynamics to the Coulomb collisions), the first set of results we present in this report is for a weakly collisional regime $\nu_{e*} \ll 1$ in which the banana and passing particle dynamics are less modified by collisions. Instead of introducing another definition into the analytic formula to represent the effective passing particle collisionality [$\nu_{e,p} = \hat{\nu}_e/(\Delta\theta_p)^2$, where $\Delta\theta_p$ is the average pitch-angle width of the passing particle velocity space measured on the vertical plane crossing the magnetic axis $R = R_0$], we continue to use $\nu_{e*}$ and $\hat{\nu}_e = \epsilon^{3/2}\nu_{e*}$ parameters for convenience but add some necessary correction parameters. $\Delta\theta_p \simeq 0.24$ for DIII-D edge pedestal and $\simeq 0.14$ for NSTX edge pedestal. Figures 1 and 2 show the model density and temperature profiles used in the simulation in the weakly collisional DIII-D and NSTX edges, respectively, at the time of numerical observation. In this full-f study, the plasma profile evolves slowly according to the weak neoclassical transport. Initial radial plasma profile shapes for DIII-D are from the experimental Shot Number 096333, with the electron temperature at the pedestal foot raised to above the experimental value in order to keep the entire pedestal in the weakly collisional regime. For the NSTX plasma, which normally has collisional pedestal, the initial plasma profile is simply manufactured to be weakly collisional, with a similar electron density and temperature profile shapes with those in the DIII-D case and a flatter ion temperature profile shape typical of the NSTX edge plasma. In all the cases shown here, the electron magnetic drift direction is chosen to be away from the single-null X-point (or the ion magnetic drift being into the X-point), which corresponds to the usual H-mode operation at lower heating power. However, numerous cases for the opposite electron drift have also been studied for a more complete study. Figure 3 shows the radial bootstrap current profiles between $0.8 \geq \psi_N \leq 1$ in weakly collisional edge plasmas obtained from XGC0 (green curves) for DIII-D ($\nu_{e*} = 0.15$, $\hat{\nu}_e = 0.031$, and $\nu_{e,p} = 0.54$) and NSTX ($\nu_{e*} = 0.14$, $\hat{\nu}_e = 0.065$, and $\nu_{e,p} = 3.32$), compared to the results obtained from the Sauter formula (blue curves). Notice that the $\nu_{e*}$ values have been intentionally chosen to be similar between two devices, even though the effective passing particle collisionalities are widely different.

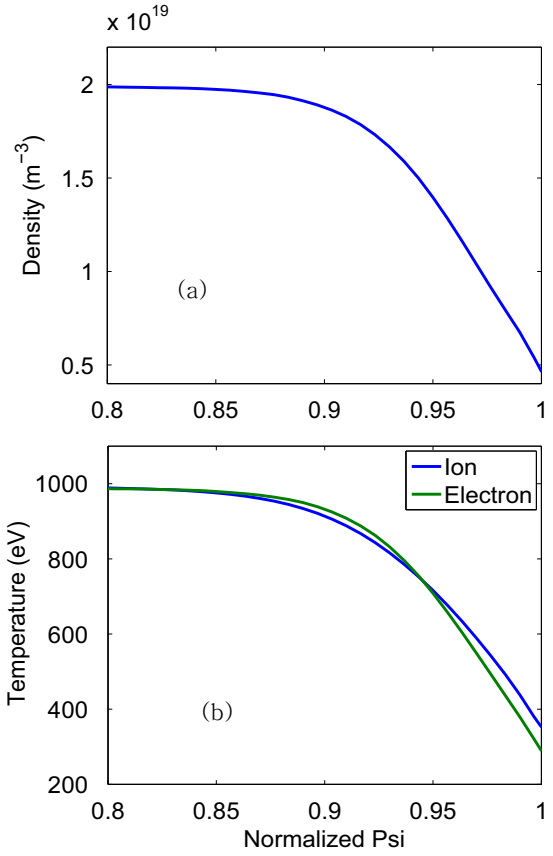


FIG. 1. Model of (a) electron density, and (b) electron and ion temperature profiles for the weakly collisional ($\nu_{e*} \ll 1$) simulation of DIII-D edge pedestal.

The average statistical error ($1/\sqrt{N}$) from total of one hundred million simulation particles is estimated to be $\sim$0.3%, based on the average number of particles per computational cell. Considering the cell-to-cell variation in the simulation particle number and cell size, the actual statistical error can be up to 1%. The Sauter formula, summarized in Sec. IV, agrees reasonably well with the XGC0 result for $\nu_{e*} \ll 1$ in both tokamaks in the radial range $\psi_N \leq 0.99$. In the DIII-D pedestal, the agreement is less than several

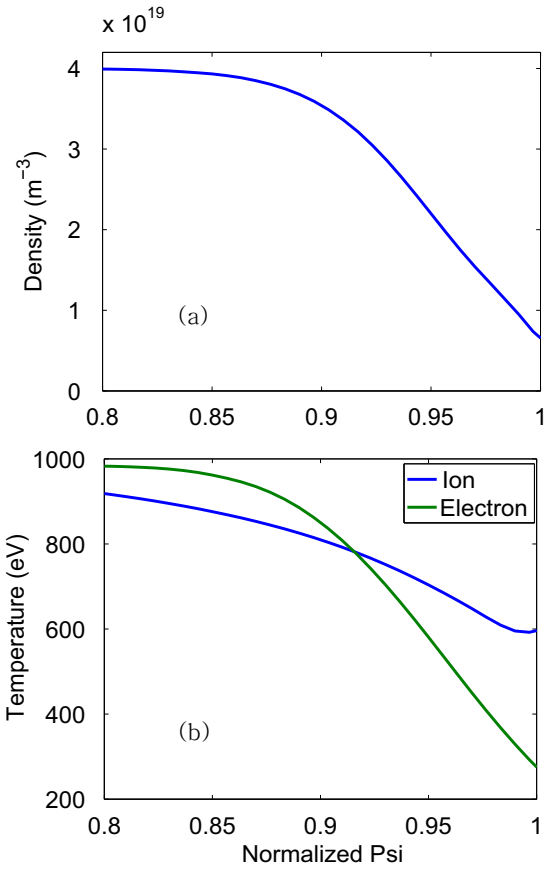


FIG. 2. Model of (a) electron density, and (b) electron and ion temperature profiles for the weakly collisional ($\nu_{e*} \ll 1$) simulation of NSTX edge pedestal.

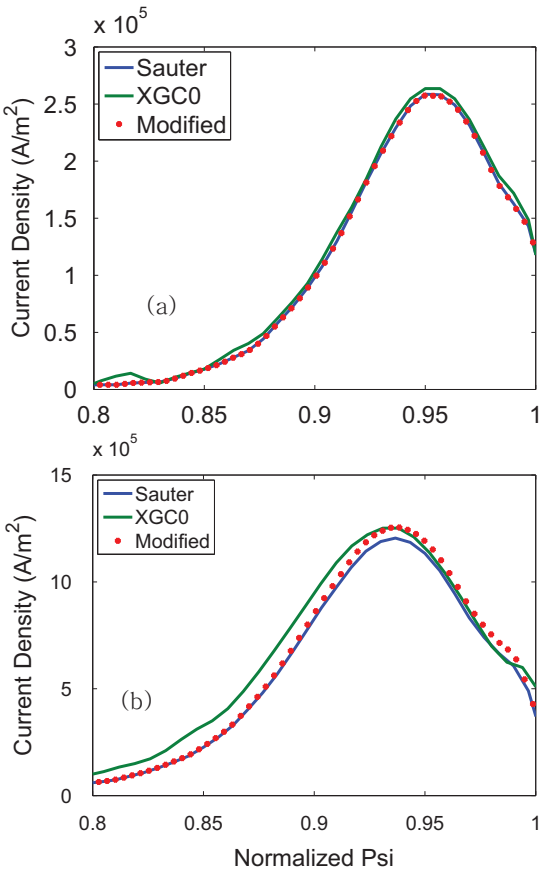


FIG. 3. Banana regime edge bootstrap current results (a) for DIII-D with $\nu_{e*} = 0.15$ at the radial position of peak bootstrap current, and (b) for NSTX with $\nu_{e*} = 0.14$. Less agreement in (b) is an indication that the passing particles in NSTX are effectively in the collisional regime. The solid blue line represents the Sauter formula and the dashed green line represents the XGC0 results. The red dots are from the modified formula, to be discussed later.

percent compared to the peak value. In the NSTX plasma edge, the agreement is worse than several percent. A little less agreement in NSTX edge plasma is not surprising since the effective passing particle collisionality $\nu_{e,p} = 3.32$ is not so low. As we lower the collision frequency further in the NSTX edge pedestal, as shown in Fig. 4, the difference between the XGC0 and Sauter formula again becomes less than several percent relative to the peak value, showing greater importance of the effective passing particle collisionality $\nu_{e,p}$ than the effective trapped particle collisionality $\nu_{e*}$. Comparison between the Sauter formula and the XGC0 result at $\psi_N > 0.99$ is less satisfactory due to the separatrix effect and is discussed in Sec. IV.

Next, we increase the electron collisionality to $\nu_{e*} \geq 5$, thus pushing the effective collisionality of the pedestal passing particles $\nu_{e,p} = \hat{\nu}_e/(\Delta\theta_p)^2$ into highly collisional regime. It is found that the agreement with the Sauter formula begins to deteriorate as the effective passing particle collision frequency is raised to $\leqslant 1$, as shown in Fig. 3(b) by comparison with Fig. 4. Figures 5 and 6 show our model density and temperature profiles for the DIII-D and NSTX edge pedestals, respectively, for plateau-collisional regime at the time of bootstrap current measurement. For the DIII-D pedestal, the plasma density has been raised and the temperature has been lowered from Fig. 1 (DIII-D shot number 096333) in order to enhance the collisionality. For the NSTX pedestal, the natural plasma profile from experimental shot number 128013 has been modeled after. Figure 7 shows comparison of the simulation results with Sauter formula for (a) DIII-D at $\nu_{e*} \simeq 7.7$ ($\hat{\nu}_e \simeq 1.6$ and $\nu_{e,p} \simeq 28$) and (b) NSTX at $\nu_{e*} \simeq 5$ ($\hat{\nu}_e \simeq 2.3$ and $\nu_{e,p} \simeq 117$) at the radial positions where the bootstrap current peaks. In the chosen DIII-D edge pedestal model profile, the peak numerical bootstrap current is found

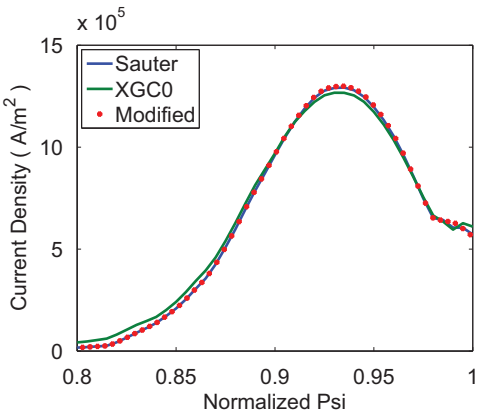


FIG. 4. Weakly collisional bootstrap current result in a NSTX edge pedestal with $\nu_{e*} = 0.017$, $\hat{\nu}_e = 0.008$, and $\nu_{e,p} = 0.41$ at the peak of bootstrap current. Solid blue line represents Sauter formula, dashed green line represents XGC0 result, and red dots represent the modified formula to be described later.

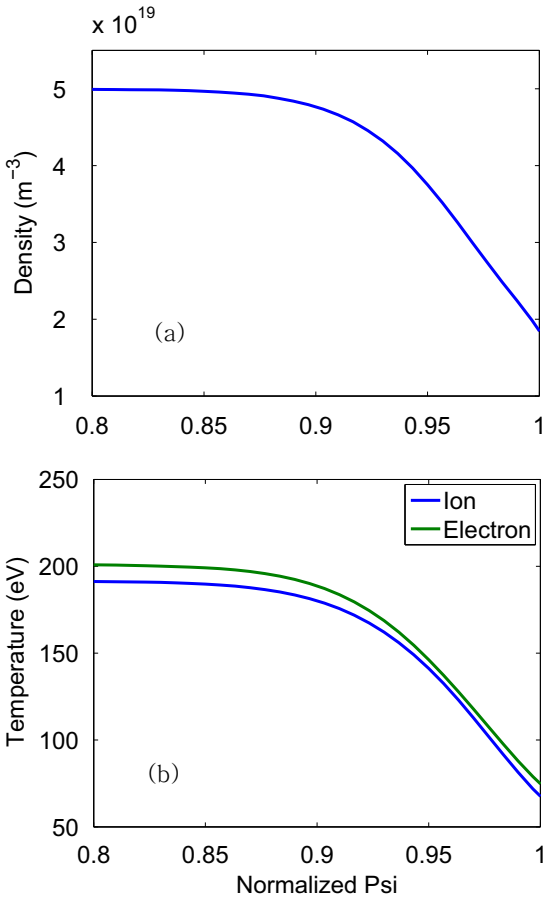


FIG. 5. Model profiles for (a) electron density, and (b) electron temperature (green solid line) and ion temperature (blue solid line) for collisional simulation of DIII-D edge pedestal.

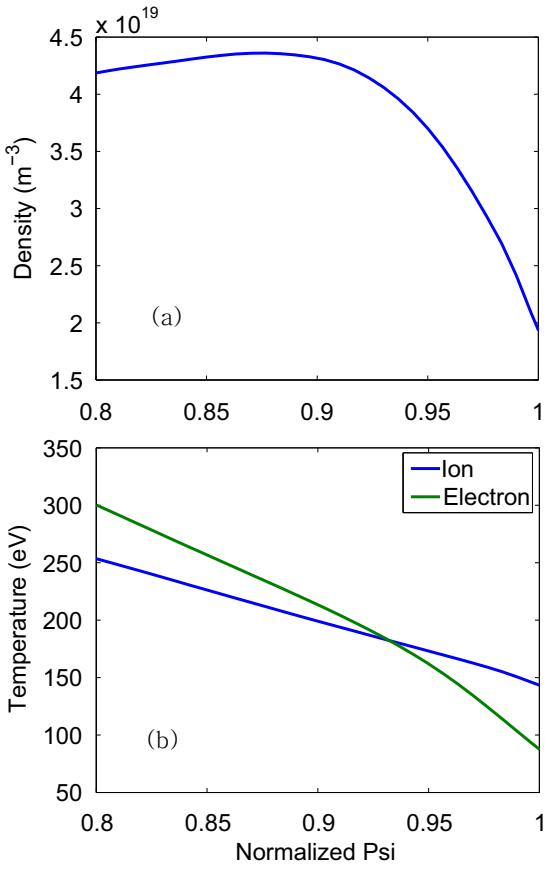


FIG. 6. Model profiles for (a) electron density, and (b) electron temperature (green solid line) and ion temperature (blue solid line) for collisional simulation of NSTX edge pedestal.

to be less than the Sauter formula result by $\sim 35\%$. In the chosen NSTX edge pedestal profile, the peak numerical value is about 50% greater than the Sauter formula result. The degree of modification from the Sauter formula depends on the plasma profile and magnetic equilibrium. Since a normal DIII-D pedestal plasma does not usually have such a high collisionality, the actual modification to the bootstrap current in DIII-D is expected to be less. For a normal NSTX edge plasma, the chosen electron collisionality is similar to a typical pedestal value, and the bootstrap current enhancement shown here is expected to be more real.

In order to examine the ion charge number effect on the bootstrap current, an artificial single main ion species is used while keeping the mass at the deuteron value but using nonunity charge numbers. This choice of one ion species, instead of using multiple ion species, is made for a faithful comparison with the Sauter formula. Figure 8 shows the electron density and temperature profiles at the time of numerical measurement for NSTX edge pedestal with the ion charge number $Z = 2$. At the bootstrap current peak, the collisionalities are $\nu_{e*} \simeq 13$, $\hat{\nu}_e \simeq 6.0$, and $\nu_{e,p} \simeq 304$. Figure 9 shows that the XGC0 result is about 70% higher than the Sauter formula in this case. As will be shown in Sec. IV, this observation reflects not only the effect of increased electron collisionality by the raised ion charge number but also some additional effect. DIII-D pedestal plasma profile with $Z = 2$ is shown in Fig. 10. At the bootstrap current peak, the collisionalities are $\nu_{e*} \simeq 7.8$, $\hat{\nu}_e \simeq 1.62$, and $\nu_{e,p} \simeq 28.4$. For this DIII-D case, Figure 11 shows that the XGC0 result is about 30% smaller than the Sauter formula.

### A. Physical interpretation of the numerical observation

In this subsection, we offer our physical interpretation of the observed numerical simulation results. The reduction in DIII-D geometry and the enhancement in NXTX geometry of the collisional pedestal bootstrap current from the existing analytic formula can be largely understood as a result of the limited reliability of the trapped-particle centered formulation of the existing theories (based upon the effective trapped particle fraction parameter), while the pedestal bootstrap current is significantly influenced by the effective passing particle fraction and the related physics. The tight-aspect-ratio NSTX geometry has an additional effect, which is different from a conventional aspect ratio geometry. Many of the trapped particles make multiple toroidal circulations at the high magnetic field side before their parallel velocity changes sign from the magnetic mirror force. At high enough effective collision frequency, these particles forget that they are in the trapped region in the velocity space and contribute to the toroidal electrical current as well as the passing particles do. The absence of the large ExB flow effect and the neglect of the large banana excursion width compared to the radial gradient scale

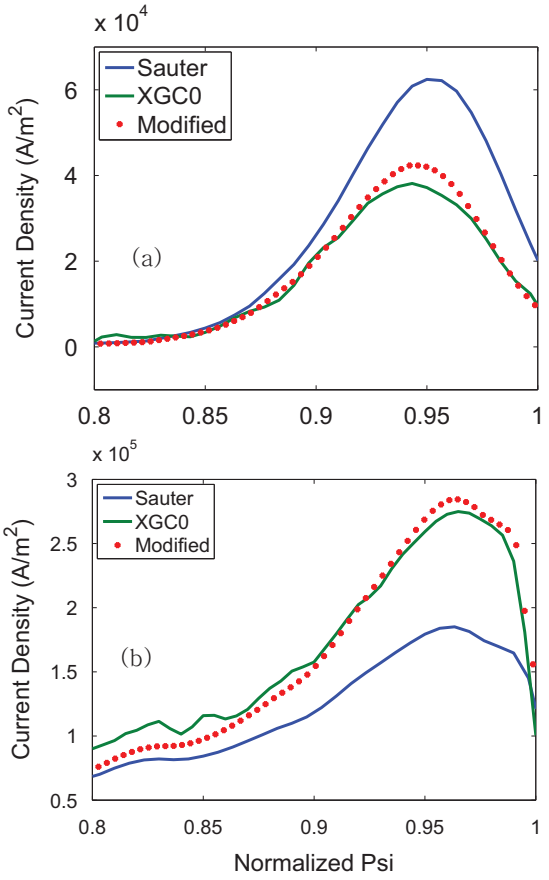


FIG. 7. Collisional bootstrap current results in edge pedestal for (a) DIII-D with $\nu_{e*} \simeq 7.7$ at the peak of bootstrap current, and (b) NSTX with $\nu_{e*} \simeq 5$. Solid blue line represents Sauter formula, dashed green line represents XGC0 result, and red dots represent the modified formula to be presented later.

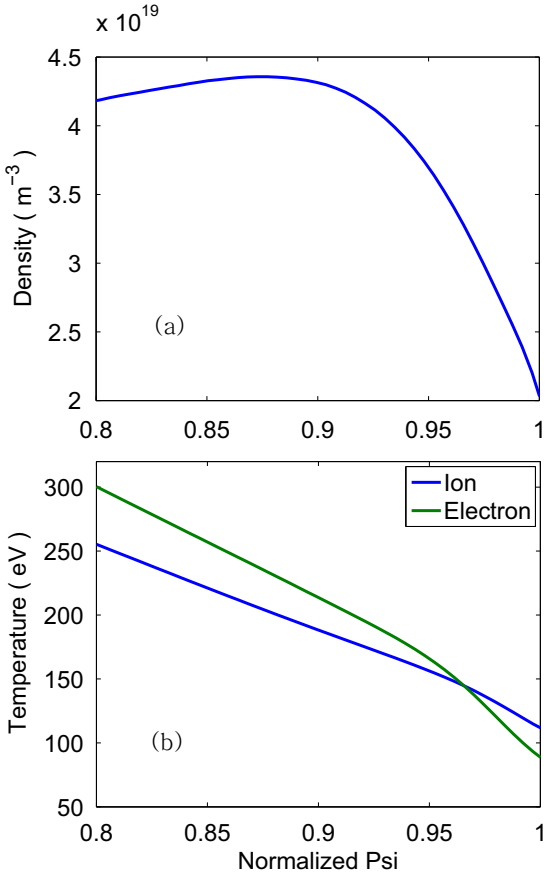


FIG. 8. Z = 2 case. (a) Electron density profile, and (b) electron and ion temperature profiles for collisional NSTX edge pedestal plasma.

length in the previous formulas could be conjectured[15] to be some additional source of discrepancy from the present kinetic simulation results, which include these effects. However, it is found numerically that these effects are insignificant compared to the effects discussed here due to the dominance of the electron contribution to the bootstrap current. The only significant finite banana effect we find is from the electron radial drift effect in contact with the magnetic separatrix surface. The Sauter formula or other such formulas do not claim validity in the edge pedestal. In fact, Fig. 7 of Ref. 10 shows steep variation of a bootstrap current coefficient with respect to edge relevant collisionality and aspect ratio, which their analytic formula could not follow. The present study has mainly focussed on the effect of edge relevant collisionality and aspect ratio on the edge bootstrap current in various case studies, even including an analytic magnetic equilibrium geometry[41] for easy variation of the flux surface shape and aspect ratio, as well as the pedestal collisionality. The present simulation study could be considered as an extension of the existing analytic formulas to the edge pedestal region in a separatrix geometry.

A trapped-passing boundary layer forms in the velocity space between the bootstrap source region (trapped particles) and the current carrier region (passing particles). This layer becomes broader with higher collisionality. In other words, in the collisional boundary layer, trapped particles spend some fraction of their orbital time as passing particles, and vice versa. The boundary layer reduces the source efficiency (and adds some carrier ability) in the trapped region and reduces the carrier efficiency in the passing region as a consequence of collisional inter-mixing of two functionalities. As a result, the effective passing fraction cannot be simply described as "1—trapped particle fractions." If so, it would

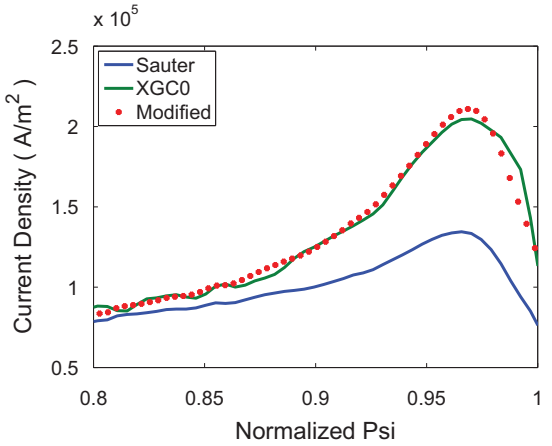


FIG. 9. Z = 2 case. Bootstrap current for NSTX collisional edge ($\nu_{e*} \simeq 13$, $\hat{\nu}_e \simeq 6.0$, and $\nu_{e,p} \simeq 304$ at the peak of bootstrap current). Solid blue line represents Sauter formula, dashed green line represents XGC0 result, and red dots represent the modified formula.

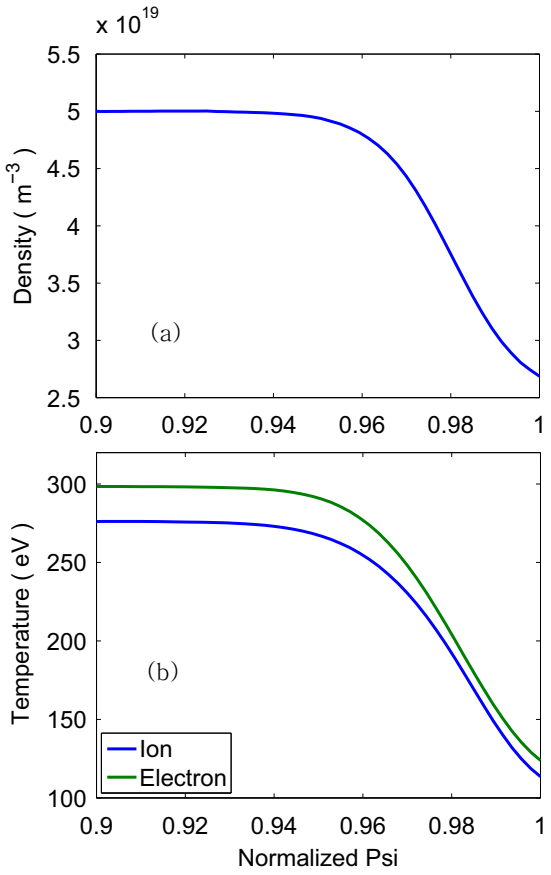


FIG. 10. Z = 2 case. (a) Electron density profile, and (b) electron and ion temperature profiles for collisional DIIID edge pedestal plasma.

have made the effective trapped particle fraction a more useful parameter in the description of the edge pedestal bootstrap current.

In the case of a conventional aspect ratio tokamak edge (represented by DIII-D in this study), there is still an adequate population of passing particles ($\Delta\theta \simeq 24\%$) to carry the current that is produced by the trapped particles. However, due to the narrowness of the passing particle region in the pitch angle space $\Delta\theta$, the effective collisionality of the passing particles $\nu_{p*}$ is greater than the effective trapped particle collisionality by the factor $\epsilon^{3/2}/(\Delta\theta)^2 \sim 3$. If the edge trapped electrons are in the so called "plateau" collisionality regime $\nu_{e*} > 1$, the passing electrons can be effectively in the collisional regime $\nu_{ep*} \gg 1$, and their current-carrying ability is reduced. Collisional reduction of the effective current carrier fraction (which decreases the bootstrap current) has not been handled properly by the "effective trapped particle fraction" parameter $\nu_{e*}$ alone. This is found to be the main reason for the reduction of the bootstrap current in the plateau-collisional conventional, aspect-ratio tokamak (DIII-D) edge.

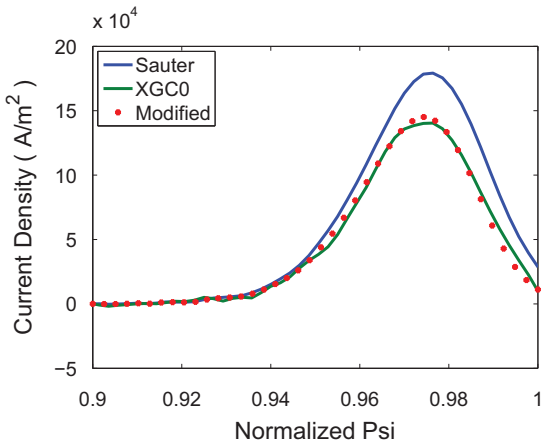


FIG. 11. Z = 2 case. Bootstrap current in a DIIID collisional pedestal ($\nu_{e*} \simeq 7.8$, $\hat{\nu}_e \simeq 1.62$, and $\nu_{e,p} \simeq 28.4$ at the peak of bootstrap current). Solid blue line represents Sauter formula, dashed green line represents XGC0 result, and red dots represent the modified formula.

In the case of a tight aspect ratio tokamak edge (represented by the NSTX in this study), on the other hand, the collisionless passing particle region in the velocity space is even narrower $\Delta\theta \simeq 14\%$, resulting in $\epsilon^{3/2}/(\Delta\theta)^2 \sim 30$. The passing particle layer, which would have contained efficient current carriers without collisions, is already destroyed when the trapped particles are in the shallow banana regime. The entire passing particles can then be easily in the collisional boundary layer. At the same time, the strong collisional boundary layer reduces the current source fraction in the trapped particle region. The previous theories and formulas capture the reductions in both the bootstrap current sources and the carriers through the use of the "effective trapped particle fraction" parameter (notice here that large effective trapped particle fraction in a tight aspect ratio tokamak still yields higher bootstrap current than that in a large aspect ratio tokamak). However, the pitch angle collisions not only reduce the passing particles' ability to carry current, but they can also enhance to some degree the current carrying ability of the trapped particles in the trapped-passing boundary layer. This feature becomes stronger in a tight aspect ratio edge, and the previous formulations in the large aspect ratio core based upon the "effective trapped particle fraction" alone do not properly capture it. The stronger collisional enhancement of the current carrying ability of the barely trapped particles in a tight aspect ratio tokamak edge can easily be understood by the fact that the trapped particles turning at the high magnetic field side of a tight aspect ratio tokamak execute a few toroidal rotations near the turning point. Under strong effective collisions, these particles forget that they are in the trapped regime and are indistinguishable from the passing particles, and carry current as well as the passing particles do. This is seen as the main reason for the enhancement of the bootstrap current in the plateau-collisional, tight aspect-ratio tokamak (NSTX) edge.

Lastly, the present kinetic simulation also confirms that the ion contribution to the bootstrap current is still insignificant ($\lesssim 10\%$) even in the edge pedestal, as has been well-known for the core bootstrap current cases. Thus, some change in the ion contribution does not affect the total bootstrap current as significantly as the electrons contribution does. The success of the Sauter formula in the weakly collisional edge pedestal region, even though it neglects the radial orbit excursion and large ExB flow effects, is found to be largely due to the smallness of the ion contribution to the total bootstrap current. The only place where the radial excursion effect makes correction to the Sauter formula in

the weakly collisional regime is in the thin radial boundary layer ($\psi_N > 0.99$, several electron banana widths from $\psi_N = 1$) in contact with the magnetic separatrix surface. Even this is the electron contribution effect.

## IV. ANALYTIC FORMULA

Given the numerical observations that the Sauter formula agrees reasonably with the present kinetic simulation result in the edge pedestal plasma as long as the electron collisionality is weak and that the electron current contribution is dominant over the ion current contribution even in the presence of strong radial electric field variation, we perform an analytic fitting as a modification to the existing Sauter formula[10]

$$\langle \vec{J}_b \cdot \vec{B} \rangle = -Ip_e \times \left( L_{31} \frac{P}{p_e} \frac{d\ln P}{d\psi} + L_{32} \frac{d\ln T_e}{d\psi} + L_{34} \alpha \frac{T_i}{ZT_e} \frac{d\ln T_i}{d\psi} \right),$$

where $I(\psi) = RB_\phi$ and $Z$ is the ion charge number.

Because the Sauter formula gives remarkably good agreement with simulation results in the deep banana regime, we maintain the functional form of the transport coefficients $L_{31}$, $L_{32}$, and $L_{34}$ to be unchanged and modify the effective trapped particle fractions $f_{teff}^{31}$, $f_{teff}^{32\_ee}$, $f_{teff}^{32\_ei}$, and $f_{teff}^{34}$ in these transport coefficients. Following Ref. 10 for the definitions of $L_{31}$, $L_{32}$, and $L_{34}$

$$\begin{aligned}
L_{31} &= F_{31}(X = f_{teff}^{31}) = \left(1 + \frac{1.4}{Z+1}\right)X - \frac{1.9}{Z+1}X^2 + \frac{0.3}{Z+1}X^3 + \frac{0.2}{Z+1}X^4, \\
f_{teff}^{31} &= \frac{f_t}{1 + (1 - 0.1f_t)\sqrt{\nu_{e*}} + 0.5(1 - f_t)\nu_{e*}/Z}, \\
L_{32} &= F_{32_ee}(X = f_{teff}^{32_ee}) + F_{32_ei}(Y = f_{teff}^{32_ei}), \\
F_{32_ee}(X) &= \frac{0.05 + 0.62Z}{Z(1 + 0.44Z)}(X - X^4) + \frac{1}{1 + 0.22Z}[X^2 - X^4 - 1.2(X^3 - X^4)] + \frac{1.2}{1 + 0.5Z}X^4, \\
F_{32_ei}(Y) &= -\frac{0.56 + 1.93Z}{Z(1 + 0.44Z)}(Y - Y^4) + \frac{4.95}{1 + 2.48Z}[Y^2 - Y^4 - 0.55(Y^3 - Y^4)] - \frac{1.2}{1 + 0.5Z}Y^4, \\
f_{teff}^{32_ee} &= \frac{f_t}{1 + 0.26(1 - f_t)\sqrt{\nu_{e*}} + 0.18(1 - 0.37f_t)\nu_{e*}/\sqrt{Z}}, \\
f_{teff}^{32_ei} &= \frac{f_t}{1 + (1 + 0.6f_t)\sqrt{\nu_{e*}} + 0.85(1 - 0.37f_t)\nu_{e*}(1 + Z)}, \\
L_{34} &= F_{31}(X = f_{teff}^{34}), \\
f_{teff}^{34} &= \frac{f_t}{1 + (1 - 0.1f_t)\sqrt{\nu_{e*}} + 0.5(1 - 0.5f_t)\nu_{e*}/Z}.
\end{aligned}$$

Here, $f_{teff}^{31}$, $f_{teff}^{32\_ee}$, $f_{teff}^{32\_ei}$, and $f_{teff}^{34}$ modify the collisionless trapped particle fraction $f_t$ by collisions:

$$f_t = 1 - \frac{3}{4}\langle B^2 \rangle \int_0^{1/B_{max}} \frac{\lambda d\lambda}{\langle \sqrt{1 - \lambda B} \rangle}.$$

It is found that an improved fit to the numerical results can be obtained by considering two edge electron effects: the separatrix effect and the narrow passing particle region effect. The separatrix effect affects the bootstrap current through the nonlocal delivery of the magnetic topology information to the flux surface of observation as a consequence of the finite banana width. Near the separatrix surface, the information delivery from the particles from outside the separatrix surface is impeded by the X-point effect as many of the electron orbits are interrupted by the diverter. Even though the figures presented in this paper are for the case of electron magnetic drift away from the single-null X-point, numerous different magnetic geometries have also been used in order to generate a more complete analytic fitting formula.

The separatrix effect is found to be not symmetric with respect to the two different electron magnetic drift directions (away or into the X-point). It is found that the separatrix effect can be accounted for by multiplying a numerical fitting factor $H(\psi)$ to the collisionless trapped particle fraction

$$f_{t,new} = f_t H(\psi), \tag{3}$$

where if the electron magnetic drift is into the X-point in a single null diverted geometry,

$$H(\psi) = 1 - (0.2/Z^4)\exp\left(-\left|\frac{\psi_s - \psi}{2.7\log(\epsilon^{1.5}\nu_{e*}/3.2 + 3)\Delta_{\psi e}}\right|\right).$$

Otherwise (including double null), $H(\psi)$ is fitted to

$$H(\psi) = 1 - (0.6/Z^4)\exp\left(-\left|\frac{\psi_s - \psi}{3.3\log(\epsilon^{1.5}\nu_{e*} + 2)\Delta_{\psi e}}\right|\right),$$

where $\psi_s$ is the value of $\psi$ at the magnetic separatrix surface, $\Delta_{\psi e}$ is the electron banana width in $\psi$ space, $\Delta_{\psi e} = (d\psi/dr)\Delta_{be} = RB_p\sqrt{\epsilon}\, m_e v_{th,e}/eB_p$ is the electron banana width in the $\psi$ space measured at the outside midplane. The $H(\psi)$ factor is more significant when the electron magnetic drift is away from the single-null X-point (which corresponds to the normal high confinement operation of a tokamak plasma). Figure 12 shows the consequence if the $H(\psi)$ factor is set to unity in the case of the electron magnetic drift away from the X-point. As can be seen from the figure, the un-corrected error by the separatrix effect is confined to a thin radial layer ($\psi_N > 0.99$) in contact with the magnetic separatrix surface, corresponding to several electron banana widths. For some theoretical considerations, the highly localized $H$-factor modification to the thin layer in contact with the separatrix surface may not be as important as the small passing particle region effect modification to be discussed below.

The small passing particle region effect is found to be modeled by modifying $f_{teff}^{3j}$ into $f_{teff,new}^{3j}$ as follows:

$$f_{teff,new}^{3j} = f_{teff}^{3j}[1 + \delta(\epsilon, \nu_{e*}, Z)], \tag{4}$$

$$\delta(\epsilon, \nu_{e*}, Z) = 0.55Z^{0.2}\left(\tanh\left(3.2\beta(\epsilon)(\epsilon^{3/2}\nu_{e*})^{1.4}/Z^{\alpha(Z)}\right) + \left(1 - \exp(-\nu_{e*}/0.1)\right) \times \tanh\left(2.2\beta(\epsilon)\epsilon^{2.8}\nu_{e*}^{0.1}/Z^{\alpha(Z)}\right)\right),$$

$$\beta(\epsilon) = Re((\epsilon - 0.44)^{0.7}),$$

where j = 1, 2, 4, and

$$\alpha(Z) = (-Z^2 + 5.998Z - 4.981)/(4.294Z^2 - 14.07Z + 12.61)$$

for $1 \le Z \le 5$ and $\alpha(Z) = 0$ for $Z > 5$.

The modified $L_{31}^{new}$, $L_{32}^{new}$, and $L_{34}^{new}$ then become

$$L_{31}^{new} = F_{31}(X = f_{teff,new}^{31}) = \left(1 + \frac{1.4}{Z+1}\right)X - \frac{1.9}{Z+1}X^2 + \frac{0.3}{Z+1}X^3 + \frac{0.2}{Z+1}X^4,$$

$$f_{teff,new}^{31} = \frac{f_{t,new}[1 + \delta(\epsilon, \nu_{e*})]}{1 + (1 - 0.1f_{t,new})\sqrt{\nu_{e*}} + 0.5(1 - f_{t,new})\nu_{e*}/Z},$$

$$L_{32}^{new} = F_{32\_ee}(X = f_{teff,new}^{32\_ee}) + F_{32\_ei}(X = f_{teff,new}^{32\_ei}),$$

$$F_{32\_ee}(X) = \frac{0.05 + 0.61Z}{Z(1 + 0.44Z)}(X - X^4) + \frac{1}{1 + 0.22Z}[X^2 - X^4 - 1.2(X^3 - X^4)] + \frac{1.2}{1 + 0.5Z}X^4,$$

$$F_{32\_ei}(Y) = -\frac{0.56 + 1.93Z}{Z(1 + 0.44Z)}(Y - Y^4) + \frac{4.95}{1 + 2.48Z}[Y^2 - Y^4 - 0.55(Y^3 - Y^4)] - \frac{1.2}{1 + 0.5Z}Y^4,$$

$$f_{teff,new}^{32\_ee} = \frac{f_{t,new}[1 + \delta(\epsilon, \nu_{e*})]}{1 + 0.26(1 - f_{t,new})\sqrt{\nu_{e*}} + 0.18(1 - 0.37f_{t,new})\nu_{e*}/\sqrt{Z}},$$

$$f_{teff,new}^{32\_ei} = \frac{f_{t,new}[1 + \delta(\epsilon, \nu_{e*})]}{1 + (1 + 0.6f_{t,new})\sqrt{\nu_{e*}} + 0.85(1 - 0.37f_{t,new})\nu_{e*}(1 + Z)},$$

$$L_{34}^{new} = F_{31}(X = f_{teff,new}^{34}),$$

$$f_{teff,new}^{34} = \frac{f_{t,new}[1 + \delta(\epsilon, \nu_{e*})]}{1 + (1 - 0.1f_{t,new})\sqrt{\nu_{e*}} + 0.5(1 - 0.5f_{t,new})\nu_{e*}/Z}.$$

Since the above correction factors are for electrons, the ion charge number $Z$ in the $\delta$ formula is equal to $Z_{eff}$. It can be easily seen that in the weakly collisional limit $\nu_{e*}^{1.4} \ll 1$ or in the large aspect ratio limit $\epsilon^{(3/2)\times 1.4} \ll 1$ (and several electron banana-width away from the magnetic separatrix surface), the modified formula reduces to the Sauter formula.

## V. INTERPRETATION OF THE SINGLE ION CHARGE Z IN TERMS OF $Z_{eff}$

As described earlier, the present model uses a single ion species with charge number $Z$, in order to be consistent with Sauter's work. In a real tokamak plasma, the hydrogenic ($Z = 1$) main ions coexist with impurity ion species. The degree of impurity contamination is conventionally described by $Z_{eff} = \sum_\beta n_\beta Z_\beta^2/n_e$, where $\beta$ represents all the ion species including the main ion species. In this section, we make a connection between $Z$ and $Z_{eff}$ in the way to best match the NCLASS simulation using multiple ion species.[7] The comparison has been made in the TRANSP code.[40] The interpretation given here applies to the ion contribution terms only, since $Z = Z_{eff}$ for the electron contributions terms as described earlier.

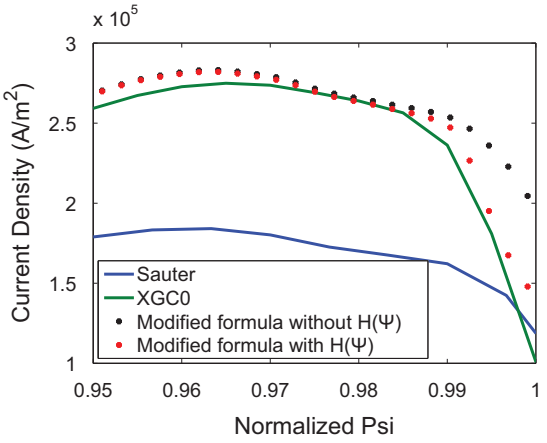


FIG. 12. Effect of the H-factor on the bootstrap current formula for the plateau-collisional NSTX pedestal case of Fig. 7. Radial domain is magnified to $0.95 < \psi_N < 1.0$. Solid blue line represents the Sauter formula, solid green line represents the XGC0 result, red dots represent the modified formula with the proper $H(\psi)$-factor, and the black dots are with $H = 1$. In this demonstration also, the electron magnetic drift is chosen to be away from the single null X-point.

For the $\alpha$ ion species with the charge number $Z_\alpha$, the collision frequency is proportional to $\nu_\alpha \propto \sum_\beta Z_\alpha^2 Z_\beta^2 \log\Lambda^{\alpha\backslash\beta}/T_\beta$, where $\beta$ includes $\alpha$ too. $Z_\alpha = 1$ for the hydrogenic main species. Using the approximation that all the ion species are thermally equilibrated to the temperature $T_i$ and that the $\log\Lambda$ is not a sensitive function of $Z_\beta$, the summation over $Z_\beta$ in the collision frequency becomes, as usual,

$$Z_\alpha^2 \sum_\beta n_\beta Z_\beta^2 = Z_\alpha^2 n_e Z_{eff}.$$

In the single ion species model used in the Sauter's and present formulas, this quantity in the ion collision frequency is identified as $n_i Z^4$, or $Z_\alpha^2 n_e Z_{eff} = n_i Z^4$. If we define an average ion charge number $\bar{Z}$ consistently with the quasi-neutrality condition $n_e \equiv n_i \bar{Z}$, and choose $n_i$ to be $n_i \equiv \sum_\beta n_\beta$, we have the relationship

$$Z_\alpha^2 n_e Z_{eff} = Z_\alpha^2 n_i \bar{Z} Z_{eff} = n_i Z^4.$$

$Z$ is then identified as

$$Z = (Z_\alpha^2 \bar{Z} Z_{eff})^{1/4}.$$

As a result, we have two different values for the charge number of the single ion species to be used in the ion part of the present formula and the original Sauter formula. $Z$ is to be used in the ion collision frequency and the quasi-neutral $\bar{Z}$ is to be used elsewhere in the ion contribution. Use of this $Z$ in the collision frequency is equivalent to the use of the actual collision frequency of the plasma with the impurity content $Z_{eff}$. There can be different choice for the $n_i$ and $\bar{Z}$ pair. The present choice for the $n_i$ and $\bar{Z}$ pair has been made from the observation that this choice makes the Sauter's bootstrap current close to the NCLASS result[7] in their most accurate common regime of banana-plateau core plasma. Other obvious choices, such as $\bar{Z} = Z$ or $Z_{eff}$, gave unsatisfactory comparison with NCLASS. For a practical tokamak plasma, realistic values $Z$ and $\bar{Z}$ are moderate ($\lesssim 2$). Carbon impurity contamination with $Z_{eff} = 4$ would yield $Z = 1.68$ and $\bar{Z} = 2$, with $n_i = n_e/2$. Such differences between the values of $Z$, $\bar{Z}$, and $Z_{eff}$ can be important in the evaluation of the Sauter single-ion definition of $\nu_{i*}$, which varies as $Z^4$.

## VI. CONCLUSION AND DISCUSSION

In the steep edge pedestal layer of H-mode (high confinement mode) tokamak plasma, a substantial bootstrap current is generated, which critically changes the equilibrium magnetic field structure and the plasma stability in the plasma edge around the magnetic separatrix. The pedestal plasma has an unconventional and difficult neoclassical property compared to the core plasma in that (1) it has a narrow passing particle region in velocity space which can be easily modified (in conventional aspect ratio tokamak) or destroyed (in a tight aspect ratio tokamak, $R_0/a \to 1$) by Coulomb collisions, that (2) it includes magnetic separatrix surface across which the topological property of the magnetic field and particle orbits change abruptly, and that (3) the ion banana width is not much smaller than the pressure gradient scale length.

A drift-kinetic particle code XGC0, equipped with a mass-momentum-energy conserving collision operator, has been used to study the bootstrap current in tokamak edge pedestal in realistic magnetic separatrix geometry under self-consistent radial electric field development. XGC0 reproduces the bootstrap formula by Sauter *et al.*[10] in the pedestal plasma with less than several percent discrepancy in the weakly collisional banana regime $\nu_{e*} \ll 1$, except in a thin layer ($\psi_N > 0.99$) in contact with the magnetic separatrix surface. This surprising result is due to the dominance of electron contribution to the bootstrap current over the ion contribution: The electron radial excursion width is much narrower than the pedestal width. The large radial electric field, and its shearing effect, on the finite ion orbit width could be important for the ion part of the bootstrap current,[15] but insignificant compared to the electron part. However, in the plateau-collisional regime $\nu_{e*} \gtrsim 1$, the XGC0-obtained bootstrap current in the steep edge pedestal can be significantly greater than the Sauter formula result in a tight aspect ratio tokamak and can be significantly smaller than the Sauter result in a conventional aspect ratio tokamak. The discrepancy arises from the sensitive collisional modification of the passing particle physics in a narrow velocity space volume, an effect did not need to be considered in the core plasma formula. A simple modification to the Sauter formula is obtained to bring the analytic fitting formula to a better agreement (within several percent accuracy compared to the peak value) with the drift-kinetic simulation results in the edge pedestal.

The electron collisionality in the edge pedestal increases rapidly as the electron temperature drops toward the magnetic separtrix. Thus, even when the electron collisionality is low at the pedestal top, the electrons in the steep gradient region (where the bootstrap current takes its peak) can be in the plateau-collisional regime. The modified formula presented

here is expected to yield an improved bootstrap current profile in the whole edge pedestal.

The present study is an extension of the existing kinetic equation solution to the edge pedestal area, utilizing a linearized Coulomb collision operator which conserves particle, momentum, and energy conserving. It is possible that a fully nonlinear Coulomb operator may change the bootstrap current solution. This question is left open. The same effect discussed here could change the edge Ohmic electrical conductivity formula or other edge neoclassical transport coefficient formulas, as extend in Ref. 42 from Ref. 10 in the conventional plasma regime. This problem is left for a future study.

## ACKNOWLEDGMENTS

This research has been funded by National R&D Program through the National Research Foundation of Korea (NRF), 2011-0018728, by SciDAC grants jointly between the US DOE Office of Fusion Energy Science and the Office of Advanced Scientific Computing Research under DE-FG02-06ER54845, by a grant from the US DOE Office of Fusion Energy Science under DE-FG02-86ER53223, and by a contract under DE-AC02-09CH11466. High performance computing time on Hopper at NERSC was made possible through NISE and ERCAP awards by US DOE.

[1]C. E. Kessel, Nucl. Fusion **34**, 1221 (1994).
[2]M. Kikuchi, M. Azumi, S. Tsuji, K. Tani, and H. Kubo, Nucl. Fusion **30**, 343 (1990).
[3]C. B. Forest, Y. S. Hwang, M. Ono, G. Greene, T. Jones, and W. Choe, Phys. Plasmas **1**, 1568 (1994).
[4]P. H. Rutherford, Phys. Fluids **16**, 1903 (1973).
[5]C. Hegna and J. D. Callen, Phys. Plasmas **1**, 2308 (1994).
[6]R. J. La Haye, Phys. Plasmas **13**, 055501 (2006).
[7]W. A. Houlberg, K. C. Shaing, S. P. Hirshman, and M. C. Zarnstorff, Phys. Plasmas **4**, 3230 (1997).
[8]S. P. Hirshman, Phys. Fluids **31**, 3150 (1988).
[9]F. L. Hinton and R. D. Hazeltine, Rev. Mod. Phys. **48**, 239 (1976).
[10]O. Sauter, C. Angioni, and Y. R. Lin-Liu, Phys. Plasmas **6**, 2834 (1999); *ibid.* **9**, 5140 (2002).
[11]R. W. Harvey and M. G. McCoy, in *Proceedings of IAEA Technical Committee Meeting on Advances in Simulation and Modeling of Thermonuclear Plasmas, Montreal, 1992* (International Atomic Energy Agency, Vienna, 1993), pp. 489–526.
[12]O. Sauter, R. W. Harvey, and F. L. Hinton, Contrib. Plasma Phys. **34**, 169 (1994).
[13]M. R. Wade, M. Murakami, and P. A. Politzer, Phys. Rev. Lett. **92**, 235005 (2004).
[14]P. B. Snyder, H. R. Wilson, J. R. Ferron, L. L. Lao, A. W. Leonard, T. H. Osborne, A. D. Turnbull, D. Mossessian, M. Murakami, and X. Q. Xu, Phys. Plasmas **9**, 2037 (2002).
[15]G. Kagan and P. J. Catto, Phys. Rev. Lett. **105**, 045002 (2010).
[16]M. C. Zarnstorff, M. G. Bell, M. Bitter, R. J. Goldston, B. Grek, R. J. Hawryluk, K. Hill, D. Johnson, D. McCune, H. Park, A. Ramsey, G. Taylor, and R. Wieland, Phys. Rev. Lett. **60**, 1306 (1988).
[17]M. Murakami, B. A. Carreras, L. R. Baylor, G. L. Bell, T. S. Bigelow, A. C. England, J. C. Glowienka, H. C. Howe, T. C. Jernigan, D. K. Lee, V. E. Lynch, C. H. Ma, D. A. Rasmussen, J. S. Tolliver, M. R. Wade, J. B. Wilgen, and W. R. Wing, Phys. Rev. Lett. **66**, 707 (1991).
[18]C. B. Forest, K. Kupfer, T. C. Luce, P. A. Politzer, L. L. Lao, M. R. Wade, D. G. Whyte, and D. Wrblewski, Phys. Rev. Lett. **73**, 2444 (1994).
[19]C. D. Challis, J. G. Cordey, H. Hamnen, P. M. Stubberfield, J. P. Christiansen, E. Lazzaro, D. G. Muir, D. Stork, and E. Thomson, Nucl. Fusion **29**, 563 (1989).
[20]K. Hoethker, H.-J. Belitz, R. P. Schorn, W. Bieger, and J. A. Boedo, Nucl. Fusion **34**, 1461 (1994).
[21]S. M. Kaye *et al.*, Nucl. Fusion **45**, S168 (2005); R. Maingi, D. P. Boyle, and J. M. Canik *et al.*, Nucl. Fusion **52**, 083001 (2012).
[22]J. L. Luxon, Nucl. Fusion **42**, 614 (2002).
[23]I. H. Hutchinson *et al.*, Phys. Plasmas **1**, 1511 (1994).
[24]G. Y. Park, C. S. Chang, I. Joseph, and R. Moyer, Phys. Plasmas **17**, 102503 (2010).
[25]C. S. Chang, S. Ku, P. H. Diamond, Z. Lin, S. Parker, T. S. Hahm, and N. Samatova, Phys. Plasmas **16**, 056108 (2009).
[26]S. Ku, C. S. Chang, and P. H. Diamond, Nucl. Fusion **49**, 115021 (2009).
[27]R. White, Phys. Fluids B **2**, 845 (1990); A. H. Boozer, *ibid.* **27**, 2441 (1984); R. G. Littlejohn, *ibid.* **28**, 2015 (1985).
[28]C. S. Chang, S. Ku, and H. Weitzner, Phys. Plasmas **11**, 2649 (2004).
[29]M. N. Rosenbluth, Bull. Am. Phys. Soc. **18**, 1337 (1973).
[30]J. W. Connor, Nucl. Fusion **13**, 221 (1973).
[31]K. T. Tsang and E. A. Frieman, Phys. Fluids **19**, 747 (1976).
[32]D. J. Sigmar, J. F. Clarke, R. V. Neidigh, and K. L. Vander Sluis, Phys. Rev. Lett. **33**, 1376 (1974).
[33]S. E. Parker, R. J. Procassini, B. I. Cohen, and C. K. Birdsall, J. Comput. Phys. **104**, 41 (1989).
[34]W. X. Wang, N. Nakajima, M. Okamoto, and S. Murakami, Plasma Phys. Controlled Fusion **41**, 1091 (1999).
[35]Z. Lin, W. M. Tang, and W. W. Lee, Phys. Plasmas **2**, 2975 (1995).
[36]X. Q. Xu and M. N. Rozenbluth, Phys. Fluids B **3**, 627 (1991).
[37]A. H. Boozer and G. Kuo-Petravic, Phys. Fluids **24**, 851 (1981).
[38]A. M. Dimits and B. I. Cohen, Phys. Rev. E **49**, 709 (1994).
[39]D. P. Stotler and C. F. F. Karney, Contrib. Plasma Phys. **34**, 392 (1994).
[40]R. J. Hawryluk, in *Proceedings of the Course in Physics of Plasmas Close to Thermonuclear Conditions, Varenna, 1979* (Commission of the European Communities, Brussels, 1980), Vol. 1, p. 19.
[41]R. L. Miller, M. S. Chu, J. M. Greene, Y. R. Lin-Liu, and R. E. Waltz, Phys. Plasmas **5**, 973 (1998).
[42]C. Angioni and O. Sauter, Phys. Plasmas **7**, 1224 (2000).

The Princeton Plasma Physics Laboratory is operated
by Princeton University under contract
with the U.S. Department of Energy.

Information Services
Princeton Plasma Physics Laboratory
P.O. Box 451
Princeton, NJ 08543

Phone: 609-243-2245
Fax: 609-243-2751
e-mail: pppl_info@pppl.gov
Internet Address: http://www.pppl.gov